

INVESTIGATION OF THE LOW POWER STAGE OF AN 1178 NM RAMAN SYSTEM

Leanne Henry, et al.

23 December 2013

Technical Paper

APPROVED FOR PUBLIC RELEASE; DISTRIBUTION IS UNLIMITED.



**AIR FORCE RESEARCH LABORATORY
Directed Energy Directorate
3550 Aberdeen Ave SE
AIR FORCE MATERIEL COMMAND
KIRTLAND AIR FORCE BASE, NM 87117-5776**

NOTICE AND SIGNATURE PAGE

Using Government drawings, specifications, or other data included in this document for any purpose other than Government procurement does not in any way obligate the U.S. Government. The fact that the Government formulated or supplied the drawings, specifications, or other data does not license the holder or any other person or corporation; or convey any rights or permission to manufacture, use, or sell any patented invention that may relate to them.

Qualified requestors may obtain copies of this report from the Defense Technical Information Center (DTIC) (<http://www.dtic.mil>).

AFRL-RD-PS-TP-2016-0010 HAS BEEN REVIEWED AND IS APPROVED FOR PUBLICATION IN ACCORDANCE WITH ASSIGNED DISTRIBUTION STATEMENT.

//LEANNE HENRY//

LEANNE HENRY, DR-III, DAF
Work Unit Manager

//KENTON WOOD//

KENTON T. WOOD, DR-IV, DAF
Chief, Laser Division

This report is published in the interest of scientific and technical information exchange, and its publication does not constitute the Government's approval or disapproval of its ideas or findings.

REPORT DOCUMENTATION PAGE				Form Approved OMB No. 0704-0188	
Public reporting burden for this collection of information is estimated to average 1 hour per response, including the time for reviewing instructions, searching existing data sources, gathering and maintaining the data needed, and completing and reviewing this collection of information. Send comments regarding this burden estimate or any other aspect of this collection of information, including suggestions for reducing this burden to Department of Defense, Washington Headquarters Services, Directorate for Information Operations and Reports (0704-0188), 1215 Jefferson Davis Highway, Suite 1204, Arlington, VA 22202-4302. Respondents should be aware that notwithstanding any other provision of law, no person shall be subject to any penalty for failing to comply with a collection of information if it does not display a currently valid OMB control number. PLEASE DO NOT RETURN YOUR FORM TO THE ABOVE ADDRESS.					
1. REPORT DATE (DD-MM-YYYY) 23-12-2013		2. REPORT TYPE Technical Paper		3. DATES COVERED (From - To) 1 Oct 2011-23 Dec 2013	
4. TITLE AND SUBTITLE Investigation of the Low Power Stage of an 1178 nm Raman System				5a. CONTRACT NUMBER In-House	
				5b. GRANT NUMBER	
				5c. PROGRAM ELEMENT NUMBER	
6. AUTHOR(S) Leanne J. Henry, **Michael Klopfer, *Cody Mart, Jake Grosek, **Ravinder Jain				5d. PROJECT NUMBER	
				5e. TASK NUMBER	
				5f. WORK UNIT NUMBER D08V	
7. PERFORMING ORGANIZATION NAME(S) AND ADDRESS(ES) *University of Arizona 163 E. University Blvd. Tucson, AZ 85721 **University of New Mexico ECE Building, Room 125 Albuquerque, NM 87131-0001				8. PERFORMING ORGANIZATION REPORT NUMBER	
9. SPONSORING / MONITORING AGENCY NAME(S) AND ADDRESS(ES) Air Force Research Laboratory 3550 Aberdeen Ave SE Kirtland AFB. NM 87117-5776				10. SPONSOR/MONITOR'S ACRONYM(S) AFRL/RDLT	
				11. SPONSOR/MONITOR'S REPORT NUMBER(S) AFRL-RD-PS-TP-2016-0010	
12. DISTRIBUTION / AVAILABILITY STATEMENT Approved for public release: Distribution unlimited. 377ABW-2013-1067, OPS-13-5738; Date 23 December 2013.					
13. SUPPLEMENTARY NOTES Presented at the Photonics West Resonator Conference 2014. "Government Purpose Rights."					
14. ABSTRACT An 1178 nm seeded and 1069 nm pumped Raman laser system where the second Stokes is amplified in a 1121 nm resonator defined by high reflector fiber Bragg gratings (FBGs) has the potential of producing high output power of narrow linewidth 1178 nm. However, 1121 nm power leakage out of the resonator cavity around the gratings was found to impact the performance of the laser and needs to be dealt with in order to obtain high 1178 nm output power levels. In order to address this problem, the causes of linewidth broadening must be understood. A fully nonlinear model has been built which involves propagation of the spectral wave shape via the nonlinear Schrödinger equation in addition to the Raman processes. It was found that increases in 1121 nm cavity power, fiber Bragg grating bandwidth, and the nonlinear index of refraction n_2 , as well as a decrease in group velocity dispersion β_2 leads to an increase in linewidth broadening. It is concluded that the magnitude of linewidth broadening seen experimentally can only be explained if the spectral components outside the bandwidth of the FBGs are being amplified. Experimentally, 1121 nm power leakage can be handled by using a three wavelength WDM on either side of the rare earth doped amplifier. In addition, usage of a fiber having a high value for group velocity dispersion and/or a low value for nonlinear index of refraction n_2 in addition to narrower bandwidth fiber Bragg gratings may help reduce the amount of linewidth broadening.					
15. SUBJECT TERMS Raman laser, resonator cavity, narrow linewidth, nonlinear Schrödinger equation					
16. SECURITY CLASSIFICATION OF:			17. LIMITATION OF ABSTRACT SAR	18. NUMBER OF PAGES 15	19a. NAME OF RESPONSIBLE PERSON Leanne Henry
a. REPORT Unclassified	b. ABSTRACT Unclassified	c. THIS PAGE Unclassified			

Investigation of the low power stage of an 1178 nm Raman system

Leanne J. Henry⁽¹⁾, Michael Klopfer⁽²⁾, Cody Mart⁽³⁾, Jake Grosek⁽¹⁾, and Ravinder Jain⁽²⁾

¹Air Force Research laboratory, Directed Energy Directorate, 3550 Aberdeen Avenue SE, Kirtland AFB, NM 87117, USA

²Department of Computer and Electrical Engineering, MSC01 1100, 1 University of New Mexico, ECE Building, Room 125, Albuquerque, NM 87131-0001

³College of Optical Sciences, University of Arizona, 1630 E. University Blvd, Tucson, AZ 85721

ABSTRACT

An 1178 nm seeded and 1069 nm pumped Raman laser system where the second Stokes is amplified in a 1121 nm resonator defined by high reflector fiber Bragg gratings (FBGs) has the potential of producing high output power of narrow linewidth 1178 nm. However, 1121 nm power leakage out of the resonator cavity around the gratings was found to impact the performance of the laser and needs to be dealt with in order to obtain high 1178 nm output power levels. In order to address this problem, the causes of linewidth broadening must be understood. A fully nonlinear model has been built which involves propagation of the spectral wave shape via the nonlinear Schrödinger equation in addition to the Raman processes. It was found that increases in 1121 nm cavity power, fiber Bragg grating bandwidth, and the nonlinear index of refraction n_2 , as well as a decrease in group velocity dispersion β_2 leads to an increase in linewidth broadening. It is concluded that the magnitude of linewidth broadening seen experimentally can only be explained if the spectral components outside the bandwidth of the FBGs are being amplified. Experimentally, 1121 nm power leakage can be handled by using a three wavelength WDM on either side of the rare earth doped amplifier. In addition, usage of a fiber having a high value for group velocity dispersion and/or a low value for nonlinear index of refraction n_2 in addition to narrower bandwidth fiber Bragg gratings may help reduce the amount of linewidth broadening.

Keywords: Raman laser, resonator cavity, narrow linewidth, nonlinear Schrödinger equation

1. INTRODUCTION

Current sodium guidestar lasers are either constructed using slab^{1,2} or fiber laser technology³⁻⁸. One way of achieving the desired output wavelength of 589 nm for sodium guidestar laser applications is through frequency doubling of 1178 nm light. Researchers at the European Southern Observatory (ESO) have been successful in constructing a narrow linewidth sodium guidestar laser based on frequency doubling of the output of a Raman fiber amplifier operating at 1178 nm³⁻⁹. The ESO reported achievement of 39 W of narrow linewidth 1178 nm or 26.5 W of 589 nm when frequency doubled. More recently, 44 W of 1 MHz linewidth 1178 nm continuous wave light was obtained by Raman amplification of a distributed feedback diode laser in a variably strained polarization-maintaining fiber with a record-high optical efficiency of 52% when pumped with a linearly polarized 1120 nm fiber laser¹⁰. Because of the all-polarization maintaining configuration, a polarization extinction ratio of 30 dB was obtained and a 20 time's reduction in the effective stimulated Brillouin scattering coefficient was achieved. A 24.3 W 589 nm laser was created from this by using an external resonant doubling cavity. Finally, 22 W of single-frequency 1178 nm was obtained from a counter-pumped two-stage Raman fiber amplifier using an acoustically tailored fiber¹¹.

In order to obtain a high power Raman laser system, it is necessary to avoid stressing the power limited components. In the past, a concept involving amplification of the pump wavelength (no signal present) with a rare earth doped amplifier that had been spliced to nested Raman cavities for amplification to higher orders was reported¹² and demonstrated by Nicholson. In this work, 81 W of output power at 1480 nm was achieved when 162 W of 1117 nm pump, was injected into a 120 m long Raman fiber. Because of the lack of seeding with the desired output wavelength, the Raman process was initiated by noise and the linewidth of the output wavelength was broad. As a follow-on to this, in 2012, Supradeepa demonstrated¹³ 104 W of 1480 nm with 220 W of pump from a similar Raman system that utilized an 1117/1175 nm wavelength division multiplexer (WDM) to avoid backward lasing at 1175 nm in the oscillator. Finally, the concept of seeding with the desired output wavelength in conjunction with an unseeded rare earth oscillator that had

been spliced onto a nested Raman resonator was presented by Mead¹⁴ in the patent literature for amplification of 1480 nm.

The goals of the work in this paper were to understand the limiting factors associated with a dual 1069 nm pump and 1178 nm signal seeded Raman laser system that involved the amplification of the second Stokes in an 1121 nm resonator cavity. Both experimental work and modeling was performed.

2. OVERVIEW OF RAMAN LASER SYSTEM

The system discussed in this article is seeded both with the zeroth Stokes pump wavelength at 1069 nm and the desired second Stokes output wavelength at 1178 nm, see Figure 1. In this system, the 1069 nm is first amplified and is then Raman converted to 1121 nm in a cavity defined by high reflector fiber Bragg gratings centered at 1121 nm. The 1178 nm signal is then amplified as it passes through the cavity. The first configuration of the system where both the 1069 and 1178 nm signals enter the system through a common WDM upstream from the ytterbium amplifier has been described in detail previously¹⁵. A reconfiguration of the original design to include the insertion of more 1178 nm isolation was deemed necessary because of a strong 1178 nm back reflection that is about -25 dB relative to the output power level, Figure 1. To enable a greater degree of isolation (70 dB) with fewer losses, the 1178 nm is injected into the laser downstream from the ytterbium doped amplifier. In addition, a 1069/1121/1178 (3 wavelength) WDM is inserted on the downstream side of the ytterbium doped amplifier to remove any residual 1121 nm propagating upstream that would favorably compete with the 1069 nm for amplification. In addition, a similar WDM is inserted on the upstream side of the amplifier to remove any 1121 nm which traversed the amplifier to avoid damage to the expensive 1069 nm source. In this system, because the fiber Bragg gratings (FBGs) are high reflectors, the 1069 nm will be Raman converted to 1121 nm which will grow in power in the 1121 nm in the resonator. The linewidth of the 1121 nm in the cavity will broaden to at a minimum, the maximum allowed by the fiber Bragg gratings. The 1178 nm seed upon entering the 1121 nm resonator cavity will then be amplified via Raman conversion of the first Stokes at 1121 nm to the second Stokes at 1178 nm. Narrow linewidth output is achievable because the system was seeded with the desired narrow linewidth output wavelength. In addition, the system is comprised of entirely polarization maintaining 10/125 fiber.

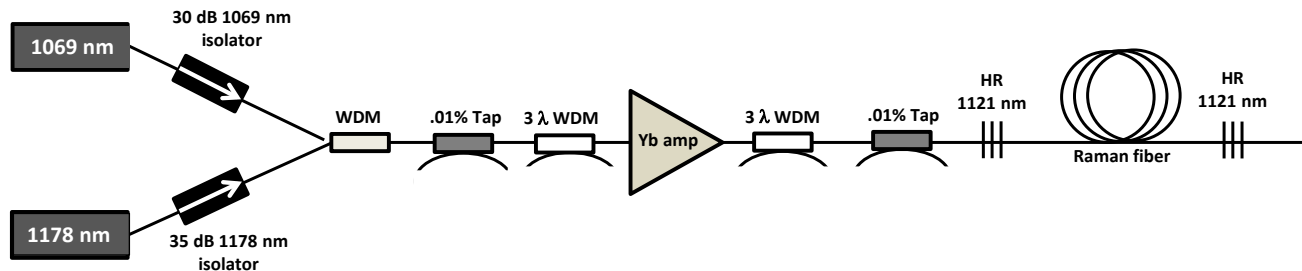


Figure 1. Schematic diagram of a single cavity Raman system that is pumped with 1069 nm and seeded with the second Stokes at 1178 nm.

3. EXPERIMENTAL RESULTS

Because of rapid growth of the 1178 nm output due to initiation of the Raman process with a seed versus noise in addition to the expected very high power levels of the first Stokes at 1121 nm in the Raman resonator, it was originally thought that a Raman fiber (either silica or germanosilicate) having a length on the order of 5-20 m, depending on the level of the 1178 nm seed, was possible. This would have been the case if the 1121nm power was building in the cavity versus leaking spectrally around the high reflector fiber Bragg gratings. Using the original configuration described in reference 15, several sets of experimental results were obtained for three different cavity lengths (11 m, 61 m, and 111 m). The fiber utilized in the cavity was Nufern FUD-4112 which is a 10/125 polarization maintaining germanosilicate fiber. For even very short cavities, an extraordinary amount of linewidth broadening of the 1121 nm in the resonator cavity, Figure 2, was observed.

The net effect of the linewidth broadening was a large amount of 1121 nm power leakage around the gratings in the spectral domain. This resulted in less buildup of 1121 nm power in the cavity than expected, i.e., it was leaking out both ends of the resonator cavity, a reduction in the conversion of 1069 nm to 1121 nm as it traversed the resonator cavity, and a lower output power of 1178 nm than expected. A longer resonator cavity was found to increase the conversion of 1069 to 1121 nm and was found to have slightly less linewidth broadening due to the lower power levels of 1121 nm in

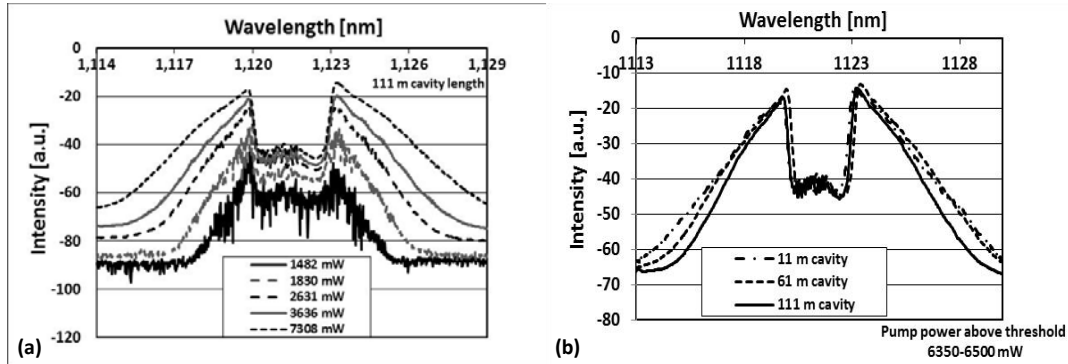


Figure 2 – (a) Linewidth broadening in 111 m cavity as a function of the 1069 nm pump power above the threshold, and (b) Linewidth broadening as a function of the cavity length.

the cavity. Although a longer cavity enabled greater Raman amplification of the 1178, the ultimate downside would be a lower threshold for SBS and ultimately, lower output power levels of 1178 nm, Figure 3. In the configuration shown in Figure 1, nearly .45 W of 1178 nm was obtained as an output prior to terminating the experiment prematurely. The big

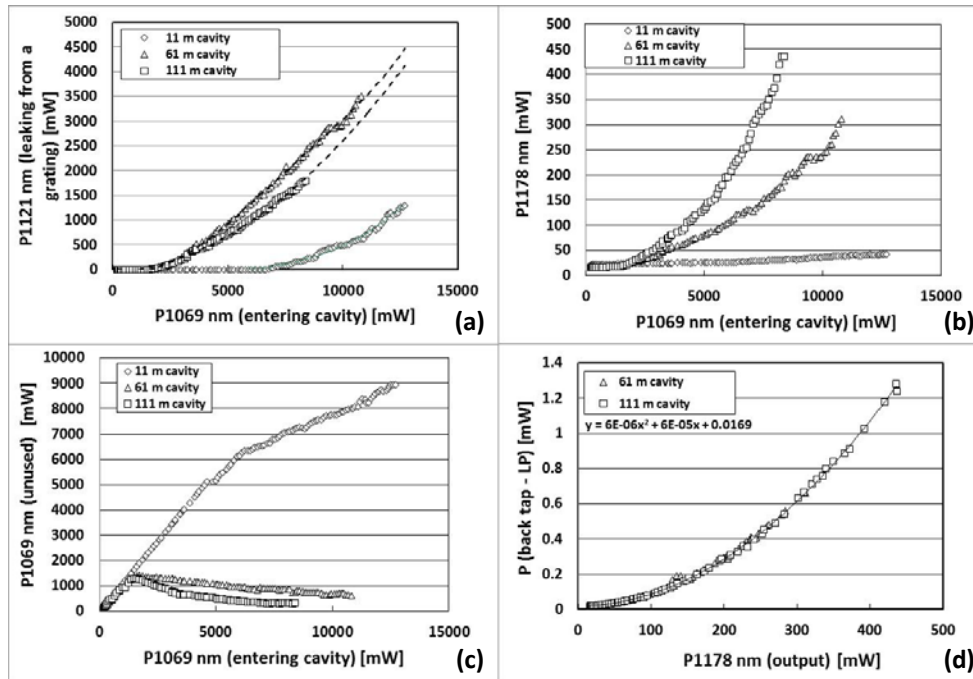


Figure 3 – (a) Leakage power level of 1121 nm from a grating, (b) Output power level of 1178 nm exiting the cavity, and (c) Unused 1069 nm ALL as a function of the power level of 1069 nm entering the resonator cavity. (d) Power out of the back tap on the lower power side of the amplifier as a function of the 1178 nm output power.

concern was the backward traversing power which was monitored out of the .01% tap coupler on the lower power side of the rare earth doped amplifier. It was found that 98.6% of the backward traveling power was 1178 nm which could be detrimental to the 1178 nm source which only had about 35 dB of isolation protecting it in this configuration. Fear of

damage to the 1178 nm source is what drove a premature stop to the experiments at less than maximum output power levels of 1178 nm. In these experiments, some linewidth broadening of the 1178 nm was seen with the 111 m cavity, see Figure 4. The amount is hard to discern because of the limited resolution of the optical spectrum analyzer.

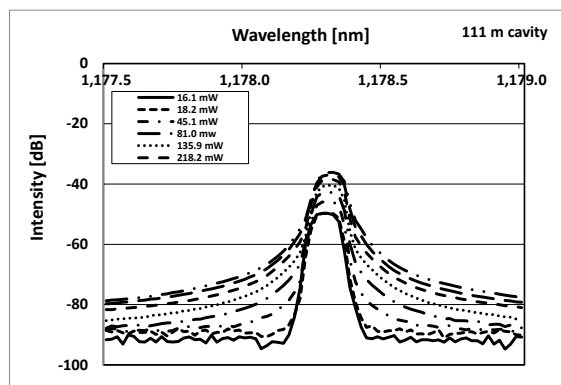


Figure 4 – Spectrum of the 1178 nm output at various power levels. At the highest output power level, about 1.66% of the 1178 nm output was initiated from noise.

To protect the 1178 nm source, the system was reconfigured as shown in Figure 1 with 70 dB of isolation protecting the 1178 nm source from the back reflection. In addition, to offset the additional losses arising from the increased isolation, the 1178 nm source was placed downstream from the ytterbium doped amplifier as far as possible. With 161 m of germanosilicate fiber comprising the cavity, an 1178 nm output of 1.1 W was obtained which was close to the threshold for Stimulated Brillouin Scattering when only one temperature zone is used. Obviously, to move forward, it is necessary to understand the driving factors behind the huge amount of 1121 nm linewidth broadening in the resonator cavity as well as how to mitigate it.

4. DESCRIPTION OF NONLINEAR MODEL

Previously a nonlinear model was developed that propagated the spectral wave shape in frequency space. This model was found to be applicable for shorter resonator cavities and for the case where the amount of linewidth broadening was somewhat limited. This was the situation since a certain minimum number of spectral points were needed to adequately

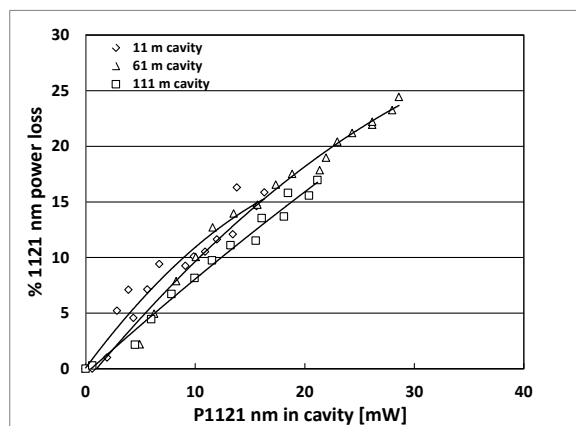


Figure 5 – Percentage of 1121 nm power leaking past a 3 nm bandwidth fiber Bragg grating having a reflectivity of 99.91% for cavity lengths of 11, 61, and 111 m.

represent the computational domain and the number of computations scaled as the number of spectral points to the fourth power. The model was found to become computationally intractable for cases involving longer resonator cavities where

there is a lot of linewidth broadening. Even with its shortcomings, this model led to some interesting insights in that longer cavities don't necessarily have increased leakage of 1121 nm power. Experimentally, the dependence on the percentage loss of 1121 nm power seemed to depend on intracavity power levels rather than the cavity length, Figure 5.

To enable investigation of a system having a lot of linewidth broadening, it is necessary to utilize the nonlinear Schrödinger equation (1) to describe the propagation of a spectral envelope down a fiber. Incorporated within the nonlinear Schrödinger equation are the following nonlinear effects: dispersion, four wave mixing, self-phase modulation, cross-phase modulation, etc. In the case of this model, the number of spectral points needed is only those necessary to adequately describe a continuous envelope in discrete space. In addition, none of the calculations scale as the number of spectral points to the fourth power.

In the present model, the spectral envelope is considered for the 1121 nm (1st Stokes) primarily because of issues associated with the huge amount of linewidth broadening in the resonator cavity. The spectral envelope is also considered for the 1178 nm (2nd Stokes) because of the importance of linewidth broadening when it comes to certain applications. The 1069 and 1242 nm are each handled as a single wavelength since linewidth broadening is not expected to be significant nor is it of interest. First, the 1121 nm spectral distribution is defined by a set of discrete spectral regions having power levels representative of the level of noise present in the system and the spectral distribution of the 1178 is assumed to be a Lorentzian representative of the seed with noise overlaid. For each distribution, the computational domain is defined to be broad enough so that effects arising from the model running up against the boundaries of the calculation are minimized. Next, the nonlinear parameter γ and the group velocity dispersion β_2 are found for the set of discrete points representing the spectral envelopes for 1121 and 1178 nm. (See references 16-19 for details on the calculation of γ and β_2 .) Once the initial spectral envelopes have been defined, the spectral envelopes for the 1121 and 1178 nm are propagated one step along the resonator cavity in the forward direction using the nonlinear Schrödinger equation and new spectral envelopes (1121 and 1178 nm) are obtained. Next, Raman is considered for the four Stokes orders involved (1069, 1121, 1178, and 1242 nm) for the same step and the power in the spectral components of both the 1121 and 1178 nm envelopes is updated based on the power and Raman gain coefficients associated with each individual component. The process just described is then repeated until the calculation reaches the end of the resonator cavity. At this point, the 1121 nm spectral envelope propagating in the forward direction is reflected off of the fiber Bragg grating and the backward traveling power in the four Stokes orders is then propagated backward along the resonator cavity using the process just described. Once the fiber Bragg grating is reached on the opposite end of the resonator cavity, the 1121 nm spectral envelope propagating in the backward direction is once again reflected and the process just described is repeated until convergence is obtained. The initial version of the code assumes that the forward and backward propagating waves do not interact with each other spectrally through the nonlinear Schrödinger equation.

The nonlinear Schrödinger equation is defined as follows^{17, 20}:

$$\frac{\partial E(z,t)}{\partial z} = (\hat{D} + \hat{N})E(z,t) \quad (1)$$

where \hat{D} is a differential operator that accounts for dispersion and losses within a linear medium, \hat{N} is a nonlinear operator that governs the effect of fiber nonlinearities on wave propagation, and $E(z,t)$ is the complex field envelope at step z and time t . \hat{D} and \hat{N} are given by:

$$\hat{D} = -\frac{\alpha}{2} - \sum_{m=2} \frac{i^{m-1}}{2^{m-1}} \beta_m \frac{\partial^m}{\partial t^m} \quad (2)$$

and

$$\hat{N} = i\gamma \left(|E(z,t)|^2 + \frac{2i}{\omega_0 E(z,t)} \frac{\partial}{\partial t} (|E(z,t)|^2 E(z,t)) \right) \quad (3)$$

where α is the absorption coefficient, β_m are the dispersion parameters of various orders, and γ is a nonlinear parameter associated with the fiber involved. The angular frequency at the center of the envelope is given by ω_0 .

For a step along the resonator cavity in z , both the linear and nonlinear parts of the nonlinear Schrödinger equation, separately, have analytical solutions but the nonlinear Schrödinger equation as a whole does not have a general analytical solution. If the step size h taken along z is small enough, then the two parts of the nonlinear Schrödinger equation can be treated separately with only a “small” numerical error that is second order in the step size h . That is,

$$E(z + h, t) \approx \exp(h\hat{D}) \cdot \exp(h\hat{N}) \cdot E(z, t). \quad (4)$$

For the nonlinear part of the nonlinear Schrödinger equation: $\frac{\partial E_N}{\partial z} = i\gamma|E|^2 E = \hat{N}E$, one obtains the following analytic solution for a small step h in the z direction:

$$E_N(z + h, t) = \exp(i\gamma|E(z, t)|^2 h) E(z, t) = \exp(h\hat{N})E(z, t). \quad (5)$$

This is considered to be an intermediate result that is not representative of the time domain at the end of a step of length h . In order to obtain a final result, dispersion must be considered. The dispersion step has an analytical solution in the frequency domain so it is necessary to first Fast Fourier transform $E_N(z + h, t)$ into the frequency domain. Also, the dispersion operator has the following form when represented in the frequency domain:

$$\hat{D}(i\omega) = \mathcal{F}\{\hat{D}\} = -\frac{\alpha}{2} - \sum_{m=2} \frac{i^{m-1}}{2^{m-1}} \beta_m (i\omega)^m. \quad (6)$$

Since the system is continuous wave, only the absorption α and the group velocity dispersion β_2 are considered in $\hat{D}(i\omega)$. Third order and higher dispersion parameters are ignored. The solution to the linear part of the nonlinear Schrödinger equation in the frequency domain: $\frac{\partial \tilde{E}_D}{\partial z} = \hat{D}(i\omega)\tilde{E}$ at the end of a step of length h therefore has the following form:

$$\tilde{E}(z + h, \omega) = \exp(h\hat{D}(i\omega))\mathcal{F}(\exp(h\hat{N})E(z, t)). \quad (7)$$

Upon Fourier transforming this result into the time domain, a representation of the time domain at the end of the step of length h is obtained:

$$E(z + h, t) = \mathcal{F}^{-1}(\tilde{E}(z + h, \omega)). \quad (8)$$

Equations (7) and (8) are therefore considered to be final results representative of the frequency and time domains at the end of a step of length h .

After the 1121 and 1178 nm spectral envelopes have been propagated a step of size h along the resonator cavity using the nonlinear Schrödinger equation, the Raman process is then applied to the same step for the four Stokes orders involved and the resultant increments in power are spread over the 1121 and 1178 nm spectra at the end of the step. For the Raman calculation, the total power in the 1121 and 1178 nm spectra is rolled up into the center wavelength of each spectral distribution. An effective Raman gain coefficient representative of each spectrum is also calculated for the 1121 and 1178 nm. Once this has been accomplished, the equations shown below for each Stokes order involved are used to propagate the power a step h along the Raman resonator¹⁷:

$$\frac{dP_{1069}^{\pm}}{dz} = \mp \frac{\lambda_{1121}}{\lambda_{1069}} \cdot \gamma_{1069} \cdot P_{1069}^{\pm} \cdot \left(\frac{P_{1121}^{\pm}}{A_{1069||1121}} \right) \mp \frac{\lambda_{1121}}{\lambda_{1069}} \cdot \gamma_{1069}^{BS} \cdot P_{1069}^{\pm} \cdot \left(\frac{P_{1121}^{\mp}}{A_{1069||1121}} \right) \mp \alpha_{1069} \cdot P_{1069}^{\pm} \quad (9)$$

$$\begin{aligned} \frac{dP_{1121}^{\pm}}{dz} = & \pm \gamma_{1069} \cdot P_{1121}^{\pm} \cdot \left(\frac{P_{1069}^{\pm}}{A_{1069||1121}} \right) \pm \gamma_{1069}^{BS} \cdot P_{1121}^{\pm} \cdot \left(\frac{P_{1069}^{\mp}}{A_{1069||1121}} \right) \mp \frac{\lambda_{1178}}{\lambda_{1121}} \cdot \gamma_{1121} \cdot P_{1121}^{\pm} \cdot \left(\frac{P_{1178}^{\pm}}{A_{1121||1178}} \right) \\ & \mp \frac{\lambda_{1178}}{\lambda_{1121}} \cdot \gamma_{1121}^{BS} \cdot P_{1121}^{\pm} \cdot \left(\frac{P_{1178}^{\mp}}{A_{1121||1178}} \right) \mp \alpha_{1121} \cdot P_{1121}^{\pm} \end{aligned} \quad (10)$$

$$\begin{aligned} \frac{dP_{1178}^{\pm}}{dz} = & \pm \gamma_{1121} \cdot P_{1178}^{\pm} \cdot \left(\frac{P_{1121}^{\pm}}{A_{1121||1178}} \right) \pm \gamma_{1121}^{BS} \cdot P_{1178}^{\pm} \cdot \left(\frac{P_{1121}^{\mp}}{A_{1121||1178}} \right) \mp \frac{\lambda_{1242}}{\lambda_{1178}} \cdot \gamma_{1178} \cdot P_{1178}^{\pm} \cdot \left(\frac{P_{1242}^{\pm}}{A_{1178||1242}} \right) \\ & \mp \frac{\lambda_{1242}}{\lambda_{1178}} \cdot \gamma_{1178}^{BS} \cdot P_{1178}^{\pm} \cdot \left(\frac{P_{1242}^{\mp}}{A_{1178||1242}} \right) \mp \gamma_B \cdot P_{1178}^{\pm} \cdot P_{SBS}^{\mp} \mp \alpha_{1178} \cdot P_{1178}^{\pm} \end{aligned} \quad (11)$$

$$\frac{dP_{1242}^{\pm}}{dz} = \pm \gamma_{1178} \cdot P_{1242}^{\pm} \cdot \left(\frac{P_{1178}^{\pm}}{A_{1178||1242}} \right) \pm \gamma_{1178}^{BS} \cdot P_{1242}^{\pm} \cdot \left(\frac{P_{1178}^{\mp}}{A_{1178||1242}} \right) \mp \alpha_{1242} \cdot P_{1242}^{\pm} \quad (12)$$

$$\frac{dP_{SBS}^{\pm}}{dz} = \pm \gamma_B \cdot P_{SBS}^{\pm} \cdot \left(\frac{P_{1178}^{\mp}}{A_{1178||1178}} \right) \mp \alpha_{SBS} \cdot P_{SBS}^{\pm}. \quad (13)$$

In these equations, the upper sign in each “+/-” refers to the forward propagating wave and the lower sign refers to the backward propagating wave. Also, γ_p refers to the Raman gain coefficient for a pump wavelength of p nm. Note that $\gamma_p = g_R \cdot \frac{1000 \text{ nm}}{p \text{ nm}}$ scales inversely with the pump wavelength and the g_R in this equation refers to the Raman gain coefficient for a pump wavelength of 1 micron. In addition, P_s^{\pm} refers to the forward/backward propagating power in the LP01 mode at s nm, γ_p^{BS} refers to the back-scattered Raman gain coefficient at a pump wavelength of p nm which is taken to be equivalent to γ_p , γ_B is the SBS coupling factor, α_s is the absorption coefficient at s nm and A_{ij} refers to the effective area for modal overlap of the pump and signal wavelengths at p and s nm.

Once the Raman calculation has been performed and the increase or decrease in power is known for each Stokes order, for the 1121 and 1178 nm, the increment in power is then spread over the discrete point's representative of the spectral envelope prior to the next step with the nonlinear Schrödinger equation. The Raman gain coefficient at the center

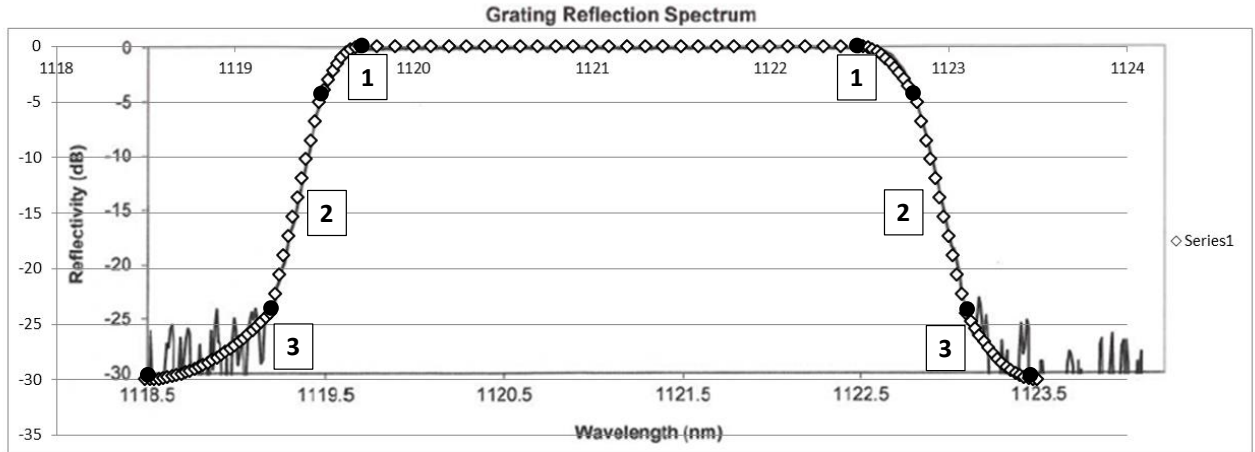


Figure 6 – Reflectivity of Teraxion fiber Bragg grating used in the experiment. The three analytic regions on the long and short wavelength sides are labeled.

wavelength of each discrete spectral region along with the power in each region determines how the increment in power is spread across each spectrum.

Finally, once the end of the resonator cavity has been reached, the power in 1121 nm will be reflected according to the reflectivity profile of the grating used in the experiment, Figure 6. The reflectivity at the other Stokes orders is assumed to be negligible in the current version of the model. The reflectivity profile of the fiber Bragg grating was modeled by fitting both the long and short wavelength sides with three functions, two second order polynomials for regions 1 and 3 and a linear function for region 2. In the model, the red points can be specified to enable investigation of the effect of various FBG edge reflectivity profiles on linewidth broadening. When a spectral envelope reflects off of a fiber Bragg grating, it is assumed that the envelope reflects according to the reflectivity characteristics of the FBG. After the power is reflected from a grating, the power in the Raman components is then reassigned to the backward propagating components in order to enable propagation of the four Stokes orders in the opposite direction. The process just described is repeated as the light propagates backward in the Raman resonator. Upon reflection off of the other grating, the entire process is repeated until convergence is obtained.

4.1 Results of the model

In order to gain an understanding of what impacts linewidth broadening, the effect of the following on the amount of linewidth broadening associated with a cavity of length 150 m was investigated by the model: 1. the group velocity dispersion β_2 , 2. the nonlinear index of refraction n_2 , 3. the 1121 nm power in the cavity, and 4. the high reflectivity

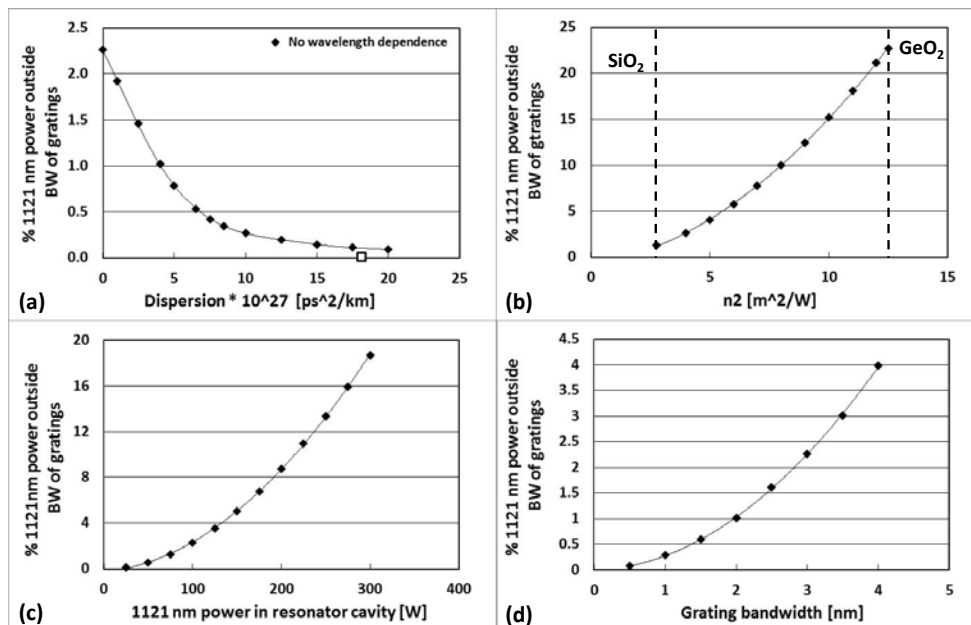


Figure 7 – (a) Effect of the group velocity dispersion on linewidth broadening, (b) Effect of the nonlinear of index of refraction n_2 on linewidth broadening, (c) Effect of 1121 nm cavity power on linewidth broadening, (d) Effect of the grating bandwidth on linewidth broadening ALL as determined by the percentage of 1121 power beyond the bandwidth of the gratings. Note that the following parameters were associated with the calculation for each case: (a) 100 W 1121 nm cavity power, 3 nm bandwidth gratings, $n_2 = 3.73 \times 10^{-20}$ m²/W (the value for a 10% germanium doped fiber core), $h = .25$ m calculation step (note that no wavelength dependence of β_2 was considered in this calculation except for the case that was specific to the fiber involved – square), (b) 100 W 1121 nm cavity power, 3 nm bandwidth gratings, $\beta_2 = 0$, $h = .25$ m, (c) 3 nm bandwidth gratings, $\beta_2 = 0$, $n_2 = 3.73 \times 10^{-20}$ m²/W, $h = .25$ m, and (d) 100 W 1121 nm cavity power, $\beta_2 = 0$, $n_2 = 3.73 \times 10^{-20}$ m²/W, $h = .25$ m. The cavity length was 150 m for all cases.

bandwidth of the FBG, see Figure 7. Since the spectrum is effectively reset at each reflection to that contained within the bandwidth of the FBG, one pass through the cavity is representative of the amount of linewidth broadening in the resonator cavity if the forward and backward propagating waves are assumed not to interact spectrally through the nonlinear Schrödinger equation. As is widely known, more linewidth broadening occurs when the value of the group velocity dispersion is low versus high. This is the case because the phase matching condition associated with four wave

mixing is broken when the value associated with the group velocity dispersion high. In order to get a feel for the maximum amount of linewidth broadening that is achievable, the group velocity dispersion was taken to be zero when investigating the effect of n_2 , the 1121 nm cavity power, and the bandwidth of the grating on the linewidth broadening. As can be seen in Figure 7, the following tends to result in increased linewidth broadening: 1. an increase in n_2 , i.e., more germanium in the fiber core, 2. a greater 1121 nm cavity power, 3. a longer cavity length, 4. a greater bandwidth of the fiber Bragg grating, and 5. a lower value of the group velocity dispersion. Of particular note is that when a realistic, wavelength dependent value was used for the group velocity dispersion, linewidth broadening was significantly reduced.

Illustration of the amount of linewidth broadening as a function of the distance traversed along a resonator cavity along with the spectral shape of the power after traversing a 150 m fiber is shown in Figure 8 as a function of the intracavity power level of 1121 nm. As expected, the amount of linewidth broadening as a function of distance traversed increased faster than linear for all 1121 nm intracavity power levels. In addition, the amount of spectral broadening also increased as the 1121 nm intracavity power level increased. Similar trends are seen for changes in n_2 , the bandwidth of the FBGs

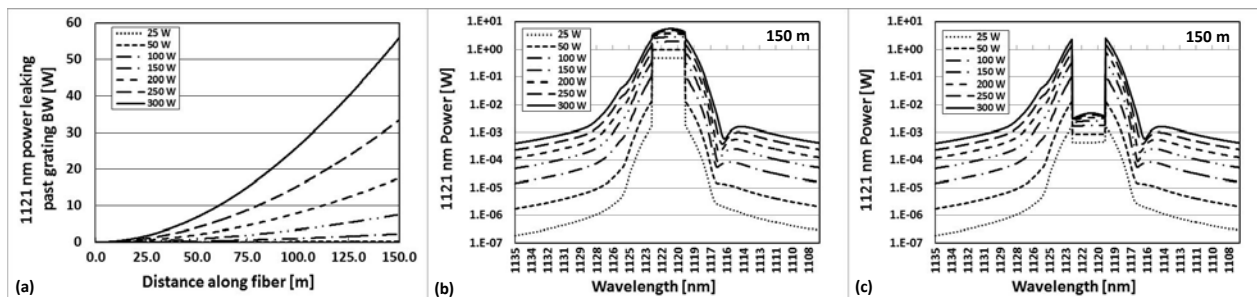


Figure 8 – (a) Amount of 1121 nm power leakage outside the high reflectivity spectral bandwidth of the FBG as a function of the distance traversed along the cavity, (b) Spectral composition of the 1121 nm power in the cavity after traversing 150 m along the cavity as a function of the 1121 nm power in the cavity, and (c) Spectral composition of the 1121 nm power which leaks past a FBG having a reflectivity of 99.91% and a 3 nm bandwidth. Note that $\beta_2 = 0$, $n_2 = 3.73 \times 10^{-20} \text{ m}^2/\text{W}$, $h = .25 \text{ m}$, and the bandwidth of the grating was 3 nm.

and the group velocity dispersion. The bottom line is that for the parameters associated with the experiment, i.e., cavity lengths of 11 to 111m, 10% germanium doping of the core which results in an $n_2 = 3.73 \times 10^{-20} \text{ m}^2/\text{W}$, wavelength dependent β_2 having a value of $1.811 \times 10^{26} \text{ ps}^2/\text{km}$ at 1121 nm, 3 nm bandwidth FBGs, and intracavity 1121 nm power levels of 17-30 W (depending on the cavity length being studied), even with β_2 taken to be zero which is not physically real, the amount of linewidth broadening seen experimentally (up to 16-25% 1121 power leakage past each grating depending on the cavity length) can't be duplicated. The fact that β_2 has a wavelength dependence and is nonzero, tends

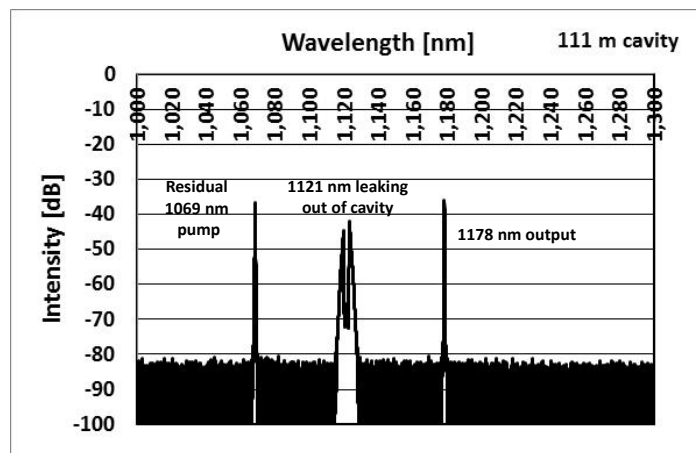


Figure 9 – Spectrum of power emerging from a 111 m cavity between 1000 and 1300 nm.

to limit the amount of linewidth broadening on a single trip up the fiber quite dramatically. In addition, experimentally, for one pass through the cavity, very little linewidth broadening was seen for the 1069 nm whereas for the 1121 nm which is effectively reset spectrally after each reflection from a FBG and therefore effectively travels the same distance, this was not the case, Figure 9. Because of the dramatic amount of linewidth broadening seen, something else is obviously occurring to support and enable amplification of 1121 nm spectral components outside the high reflectivity bandwidth of the FBG. Some possibilities are: 1. Spectral interaction of 1121 nm power propagating in one direction with power propagating in the other direction in the resonator cavity, i.e., the power reflecting off of a grating which has been spectrally narrowed would see power propagating in the opposite direction which has been broadened due to propagation along the cavity since the system is continuous wave, 2. Residual reflectivity of power out beyond the high reflectivity bandwidth of the grating, or 3. A scattering process at the fiber Bragg grating.

The effect on linewidth broadening due to an increased baseline reflectivity out beyond the high reflectivity bandwidth of the fiber Bragg gratings was investigated. Note that data from the manufacturer, Figure 6, seems to indicate a reflectivity in these regions of -25 to -30 dB. The fall off of the FBG reflectivity to baseline was assumed to occur over a 0.2 nm range on either side of the high reflectivity part of the grating for modeling purposes. The following case was considered: 11 m cavity, 3 nm FBGs, $\beta_2 = 0$, $n_2 = 3.73 \times 10^{-20}$, $h = .5$ m, 1069 nm input power of 40W, 1178 nm input

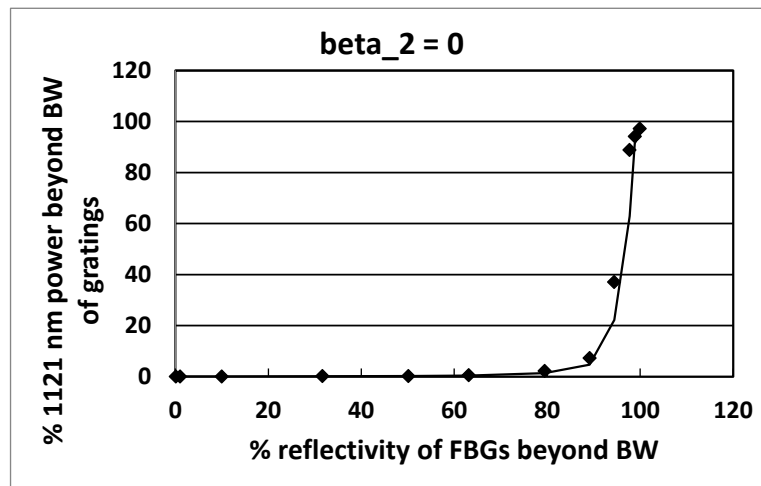


Figure 10 – Percentage of cavity power leaking past a fiber Bragg grating in the forward direction versus the percentage reflectivity of the fiber Bragg grating beyond the high reflectivity bandwidth. The case considered was: 11 m cavity, 40 W 1069 nm, 1 W 1178 nm, 3 nm bandwidth FBGs, $\beta_2 = 0$, $n_2 = 3.73 \times 10^{-20}$, $h = .5$ m, 186 nm of calculational bandwidth, and fall off of grating reflectivity over .2 nm range on either side of grating.

power of 1 W, and 186 nm of calculational bandwidth. Multiple passes of the light through the resonator cavity was simulated until convergence was achieved. As can be seen in Figure 10, the percentage of 1121 cavity power residing outside the high reflectivity bandwidth of a FBG increased quite dramatically once the baseline reflectivity of the FBG reached greater than 80 percent. (Note that the usage of $\beta_2 = 0$ is the high linewidth broadening case.) Because the baseline reflectivity of the FBGs used in the experiment was in the neighborhood of -20 to -30 dB according to the specifications and measurements of the supplier, the residual reflectivity of the 1121 nm spectral components outside the high reflectivity bandwidth of a FBG is not the source of the tremendous amount of linewidth broadening observed experimentally, i.e., calculations using residual reflectivities of -20 to -30 dB do not support this.

5. CONCLUSION

The leakage of 1121 nm power from the resonator cavity is a problem that needs to be dealt with in order to obtain high output power levels of 1178 nm. Experimentally, 1121 nm power leakage can be handled by using a three wavelength WDM on either side of the rare earth doped amplifier. In addition, usage of a fiber having a high value for the group velocity dispersion and/or a low value for the nonlinear index of refraction n_2 would probably lead to less linewidth

broadening. In addition, the usage of narrower bandwidth FBGs might help as well. Finally, additional development of the model is necessary in order to gain a full understanding of the source of the linewidth broadening in the 1121 nm resonator cavity. In particular, the investigation of the effect of a spectral interaction between the forward and backward propagating waves in the resonator cavity is necessary in conjunction with a more realistic representation of the fiber Bragg gratings. To conclude, 1121 nm power leakage from the resonator cavity will probably drive the usage of a longer Raman cavity than previously planned since lower 1121 nm cavity power levels leads to reduced conversion of the various Stokes orders. The impact of this will be the need for mitigation of Stimulated Brillouin Scattering in order to raise the output power level of the 1178 nm.

REFERENCES

- [1] Telle, J., Drummond, J., Denman, C., Hillman, P., Moore, G., and Novotny, S., "Studies of a mesospheric sodium guidestar pumped by continuous-wave sum frequency mixing of two Nd:YAG laser lines in lithium triborate", *Proceedings of the SPIE* **6215**, 62150K-1 to 62150K-10 (2006).
- [2] Denman, C.A., Hillman, P.D., Moore, G.T., Telle, J.M., Grime, B.W., and Bienfang, J.C., "Continuous wave sodium beacon excitation source", U.S. Patent number 7,035,297, April 25, 2006.
- [3] Feng, Y., Taylor, L.R., Bonaccini Calia, D., Holzlöhner, R., and Hackenberg, W., "39 W narrow linewidth Raman fiber amplifier with frequency doubling to 26.5 W at 589 nm", presented at *Frontiers in Optics*, San Diego, postdeadline paper PDPA4 (2009).
- [4] Feng, Y., Taylor, L.R., and Bonaccini Calia, D., "25 W Raman-fiber-amplifier-based 589 nm laser for laser guidestar", *Optics Express* **17**(21), 19021-19026 (2009).
- [5] Feng, Y., Taylor, L., and Bonaccini Calia, D., "Multiwatts narrow linewidth Fiber Raman amplifiers", *Optics Express* **16**(15), 10927-10932 (2008).
- [6] Taylor, L.R., Feng, Y., and Calia, D.B., "50W CW visible laser source at 589 nm obtained via frequency doubling of three coherently combined narrow-band Raman fiber amplifiers", *Optics Express* **18**(8), 8540-8555 (2010).
- [7] Taylor, L.R., Feng, Y., Hackenberg, W., Holzlohner, R., and Bonaccini Calia, D., "Narrow band fiber Raman optical amplifier", World Intellectual Property Organization WO/2009/090096.
- [8] Taylor, L.R., Feng, Y., Hackenberg, W., Holzlohner, R., and Bonaccini Calia, D., "Narrow band fiber Raman optical amplifier", U.S. Patent Application Publication #2011/0038035 A1, Feb 17, 2011.
- [9] Taylor, L.R., Feng, Y., Hackenberg, W., Holzlohner, R., and Bonaccini Calia, D., "Narrowband fiber Raman optical amplifier", Patent application #2011/0038035 A1, Feb 17, 2011.
- [10] Zhang, L., Hu, J., Wang, J., and Feng, Y., "Stimulated -Brillouin-scattering-suppressed high-power single-frequency polarization-maintaining Raman fiber amplifier with longitudinally varied strain for laser guide star", *Optics Letters* **37**(22)(2012)4796.
- [11] Dajani, I., Vergien, C., Robin, C., and Ward, B., "Investigations of single-frequency Raman fiber amplifiers operating at 1178 nm", *Optics Express* **21**(10)(2013)12038.
- [12] Nicholson, J.W., Yan, M.F., Wisk, P., Fleming, J., DiMarcello, F., Monberg, E., Taunay, T., Headley, C. and DiGiovanni, D.J., "Raman fiber laser with 81 W output power at 1480 nm", *Optics Letters* **35**(18)(2010)3069.
- [13] Supradeepa, V.R., Nicholson, J.W., Headley, C., and Lee, Y.-W., "Cascaded Raman Fiber Laser at 1480 nm with Output Power of 104 W", *Proceedings of the SPIE* **8237**(2012)82370J.
- [14] Mead, R.D., "Spectrally beam combined laser system and method at eye-safer wavelengths", US Patent Application Publication #2011/0122482, May 26, 2011.
- [15] Henry, L.J., Grosek, J., Moore, G., and Shay, T., "1121 nm resonator properties and impact on the design of a 1178 nm sodium guidestar laser", *Proceedings of the SPIE* **8236**(2012)823605.
- [16] Kato, T., Suetsugu, Y., and Nishimura, M., "Estimation of nonlinear refractive index in various silica-based glasses for optical fibers", *Optics Letters* **20**(22)(1995)2279
- [17] Agarwal, G.P., "Nonlinear fiber optics", 4th edition, Elsevier Inc., ©2007.
- [18] Milam, D., "Review and assessment of measured values of the nonlinear refractive-index coefficient of fused silica", *Applied Optics* **37**(3)(1998)546
- [19] Okamoto, K., "Fundamentals of Optical Waveguides", 2nd edition, Elsevier, ©2006.
- [20] Washburn, "Numerical Solution to the nonlinear Schrödinger equation", Chapter 4, www.phys.ksu.edu/personal/washburn/pdf/washburn_thesis_chapter4.pdf.

DISTRIBUTION LIST

DTIC/OCP 8725 John J. Kingman Rd, Suite 0944 Ft Belvoir, VA 22060-6218	1 cy
AFRL/RVIL Kirtland AFB, NM 87117-5776	1 cy
Leanne Henry Official Record Copy AFRL/RDLT	1 cy